

Microstructural Evolution During Friction Surfacing of Austenitic Stainless Steel AISI 304 on Low Carbon Steel

H. KHALID RAFI, N. KISHORE BABU, G. PHANIKUMAR, and K. PRASAD RAO

Austenitic stainless steel AISI 304 coating was deposited over low carbon steel substrate by means of friction surfacing and the microstructural evolution was studied. The microstructural characterization of the coating was carried out by optical microscopy (OM), electron back scattered diffraction (EBSD), and transmission electron microscopy (TEM). The coating exhibited refined grains (average size of 5 μm) as compared to the coarse grains (average size of 40 μm) in as-received consumable rod. The results from the microstructural characterization studies show that discontinuous dynamic recrystallization (DDRX) is the responsible mechanism for grain evolution as a consequence of severe plastic deformation.

DOI: 10.1007/s11661-012-1366-3

© The Minerals, Metals & Materials Society and ASM International 2012

I. INTRODUCTION

FRICITION surfacing is a promising new technology for depositing metallurgically bonded coatings on engineering components to combat wear and corrosion. Being a solid-state process, friction surfacing eliminates the problems such as porosity, hot cracking, segregation, and dilution which are commonly associated with conventional fusion-based techniques. In this process, a rotating cylindrical consumable rod is fed against a substrate with axial force acting simultaneously on the rod. The frictional heat is generated between the substrate and the consumable rod. Once the rubbing end of the consumable rod is sufficiently plasticized, the substrate is traversed horizontally with respect to the vertical consumable rod. Material flow at the area of contact occurs due to the combined effect of axial load, rod rotational speed, and substrate traverse speed. As the substrate moves at a specific rate, the plasticized metal deposits over it. The vertical force consolidates the plasticized metal and results in the formation of a continuous and metallurgically bonded layer. A schematic representation of friction surfacing process is shown in Figure 1.

Realizing the potential of friction surfacing, attempts were made by many researchers to coat a variety of metallic materials on different metallic substrates by means of friction surfacing.^[1-5] They found that ferrous materials in general are readily coatable.^[1-3,5] Non-

ferrous materials pose some problems due to their high thermal conductivity and high temperature instability.^[2,4]

Among ferrous materials, stainless steels were found to be more attractive coating materials owing to their application potential as candidate materials for corrosion protection. Traditionally, stainless steel claddings were made by means of the Laser/TIG welding process. To minimize dilution and to retain material chemistry, buffer layers or highly alloyed stainless steels (like AISI 308 and AISI 309) are always used.^[6] However, it suffers from problems associated with solidification. In addition, the process is time consuming and not cost effective. Therefore, a solid-state process which does not involve melting can address these issues and friction surfacing is an ideal solid-state process which can deposit relatively thick metallic coatings.

Friction surfacing of AISI 304 was reported earlier.^[1,7] However, emphasis was on the feasibility aspects and on the effect of process parameters. Although some microstructural aspects of friction surfaced stainless steel were reported,^[4,8] detailed information on the microstructural characterization of AISI 304 friction surfaced coatings was not available in the open literature. An understanding on the microstructure and morphology of the coating is necessary as it has a direct bearing on the performance characteristics of the coating. Hence, in this work, friction surfaced AISI 304 coating is characterized by Optical microscopy (OM), Electron back scattered diffraction (EBSD), and Transmission electron microscopy (TEM) to understand the microstructural evolution during the friction surfacing process.

II. EXPERIMENTAL METHODS

Friction surfacing was carried out in a custom-developed machine. The machine was capable of delivering an axial load of 10 kN, maximum spindle rotation speed of 3000 rpm, and table traverse speed in steps of 0.1 mm/seconds. AISI 304 (chemical composition in weight percent

H. KHALID RAFI, formerly with the Department of Metallurgical and Materials Engineering, Indian Institute of Technology Madras, Chennai 600036, India, is now Post Doctoral Associate with Department of Industrial Engineering, J.B. Speed School of Engineering, University of Louisville, Louisville, KY 40292. Contact e-mail: khalidrafi@gmail.com N. KISHORE BABU, Scientist, is with the Joining Technology Group, Singapore Institute of Manufacturing Technology (SIMTech), 71 Nanyang Drive, Singapore 638075, Singapore. G. PHANIKUMAR, Associate Professor, and K. PRASAD RAO, Professor, are with the Department of Metallurgical and Materials Engineering, Indian Institute of Technology Madras.

Manuscript submitted February 20, 2012.

Article published online September 5, 2012

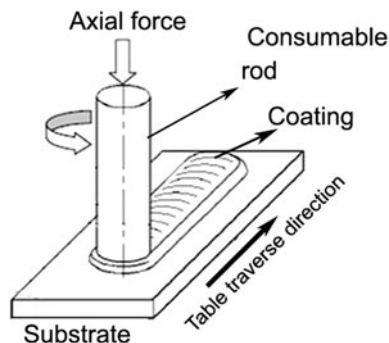


Fig. 1—Schematic of friction surfacing.

0.08 C, 17.75 Cr, 7.7 Ni, 1.17 Mn, 0.77 Si, and balance Fe) was used as the coating material/consumable rod and low carbon steel (chemical composition in weight percent 0.12 C, 0.42 Mn, 0.02 P, 0.01 S, and balance Fe) was used as the substrate material. The consumable rod used was of 100 mm length and 18 mm diameter and the dimension of the substrate plate was 200 mm × 100 mm × 10 mm. The contact end of the consumable rod and the substrate top surface were surface grinded to insure complete contact. The substrate was clamped firmly in the machine table to avoid any displacement due to vibration during the process. The surfaces were thoroughly cleaned with acetone just before the process began.

Coatings were produced by optimized parameters from a previous work done by the authors.^[9] Taguchi L8 orthogonal array design of experiments was used to optimize the process parameters. The range of parameters to carry out Taguchi experiments was identified by conducting initial trial runs. It was found from the preliminary experiments that thinner coatings can provide better strength. Hence, the parameters were optimized for coating thickness and shear strength. The optimized parameters obtained were: Axial load -10 kN, rotation speed -800 rpm, and traverse speed 4.4 mm/seconds.

Investigation on the microstructural evolution was undertaken in the coating top surface by OM, EBSD, and TEM techniques. All the characterization studies for the as-received bar material were performed in specimens prepared from the longitudinal cross-section. For the coating, the specimens were extracted from the middle of the coating by slicing the coating in horizontal plane. OM specimens were prepared following standard metallographic specimen preparation methods. EBSD specimens were mechanically ground and electrolytically polished. EBSD study was performed using a FEI QUANTA scanning electron microscope operated at 30 kV and equipped with a fully automatic HKL Technology EBSD attachment. Orientation image mapping (OIM) was performed in the normal direction to the coating surface and toward the friction surfacing direction with a scan step size of 0.25 μm. The HKL channel 5 software was used for data acquisition and post-processing. For TEM samples, disks of 3 mm diameter were ground to a thickness less than 100 μm and then twin-jet electropolished using a solution containing 5 pct perchloric acid in methanol at

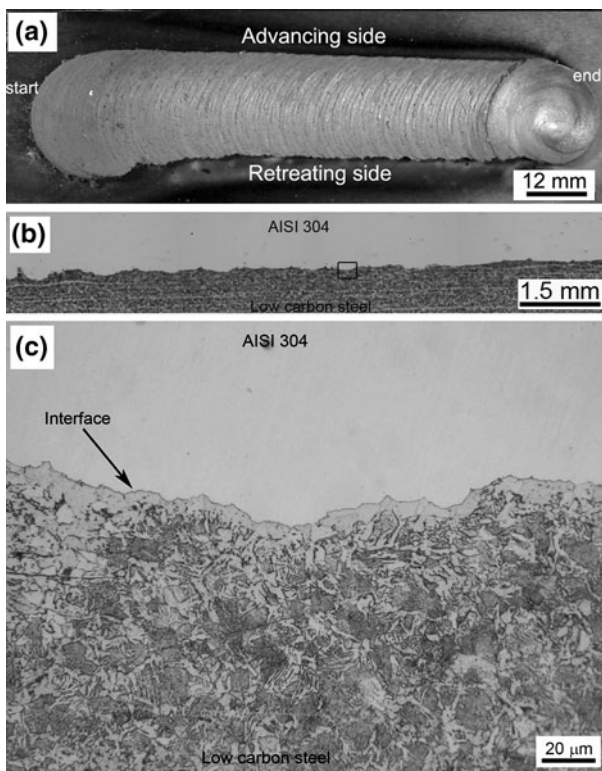


Fig. 2—(a) Friction surfaced AISI 304 coating, (b) Montage of the interface, and (c) enlarged view of boxed region in (b).

-243 K (-30 °C) and a voltage of 20 V. TEM examination of thin foils was performed using a Philips CM 20 microscope.

III. RESULTS AND DISCUSSION

The coating/substrate interface characteristics can be observed from the cross-sectional microstructure (Figure 2) which shows very good interfacial bonding. The interface is free from any defects, which indicate a proper metallurgical bonding between the coating and the substrate.

To understand the mechanism involved in the evolution of coating microstructure, microstructural characterization was carried out by EBSD and TEM. The orientation image maps shown in Figures 3(a) and (b) clearly show the scale-down in grain size between the as-received material and the coating. The colors correspond to crystallographic orientation normal to the observed sample plane as shown in the color-coded triangle (Figure 3(c)) to represent the orientation of grains. No color appears more often than any other given color, which indicates the randomness in the orientation of grains. Figures 4(a) and (b) show the characteristic pole figures corresponding to the orientations of Figures 3(a) and (b). No specific crystallographic orientation is observed as there is no accumulation of poles around a specific direction. This shows that the entire sample has a random texture.

The as-received material has an annealed coarse grain structure. Annealing twin boundaries are also observed

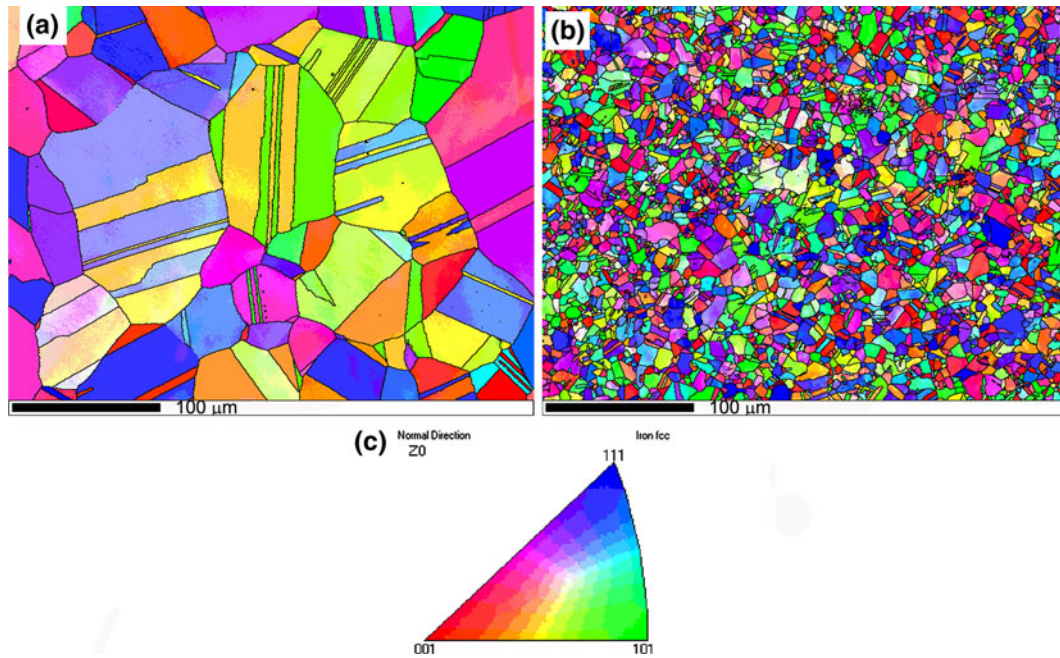


Fig. 3—EBSD orientation image maps (OIM). (a) As-received AISI 304 consumable rod, (b) friction surfaced AISI 304 coating, and (c) color-coded triangle to represent the orientation of grains.

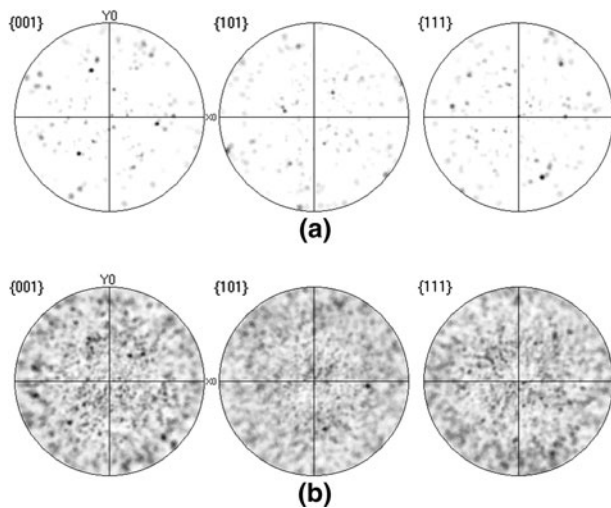


Fig. 4—(a) Characteristic pole figure corresponding to Fig. 3(a) and (b) characteristic pole figure corresponding to Fig. 3(b).

in grain interiors. The average grain size measured by the linear intercept method for all high angle boundaries is $40 \mu\text{m}$. The friction surfaced coating exhibited fine equi-axed grains. The refined microstructure has an average grain size of $5 \mu\text{m}$. The fine equi-axed grain structure is an indication of dynamic recrystallization.

The crystal orientation maps illustrate the development of typical heterogeneous discontinuous dynamically recrystallized microstructure in AISI 304 friction surfaced coatings. A wide range of grain sizes uniformly distributed throughout the material can be observed. For a better analysis of the microstructural changes due to straining, EBSD provides quantitative measurements of the low angle boundary (f_{LAB}) and twin boundary

fractions (f_{TB}). The as-received material condition is characterized by distortion-free grains, and a relatively high fraction of twin boundaries are present in almost all the grains. The f_{LAB} and f_{TB} corresponding to the misorientation angle of 60 deg around a $\langle 111 \rangle$ axis are shown in Figures 5(a) and (b). The f_{TB} in the coating is reduced to 50 pct as compared to 70 pct in the as-received material. Similarly, the histograms show an increase in the fraction of low angle boundaries for coatings, which is associated with substructure formation.

To further substantiate the grain refinement mechanism, microstructural characterization was carried out by TEM. Figures 6(a) and (b) show TEM bright field images of the as-received AISI 304 and friction surfaced AISI 304 coating, respectively. Fine grains with minimal dislocations are observed on the TEM image of coating microstructure. Given the severe plastic deformation and the associated strain rate involved in the process, the grains sizes could be even finer. But, the high temperature developed due to friction heating accelerates the grain boundary migration rate, resulting in grain coarsening. Higher magnification TEM images (Figures 7(a) through (c)) show substructures formed by preferential alignment of dislocations. This is attributed to the strain energy stored in the material during processing, which is the driving force for dynamic recrystallization (DRX). TEM studies also show that the coating is free from any carbides or secondary phases.

For metallic alloys based on copper, aluminum, nickel, and austenitic iron, which do not undergo any phase change during cooling, recrystallization after deformation is the method for refining the grain structure. Similarly, DRX is an inherent phenomenon during hot working of these metals. The mechanism of DRX is well established and, very precisely, it is the

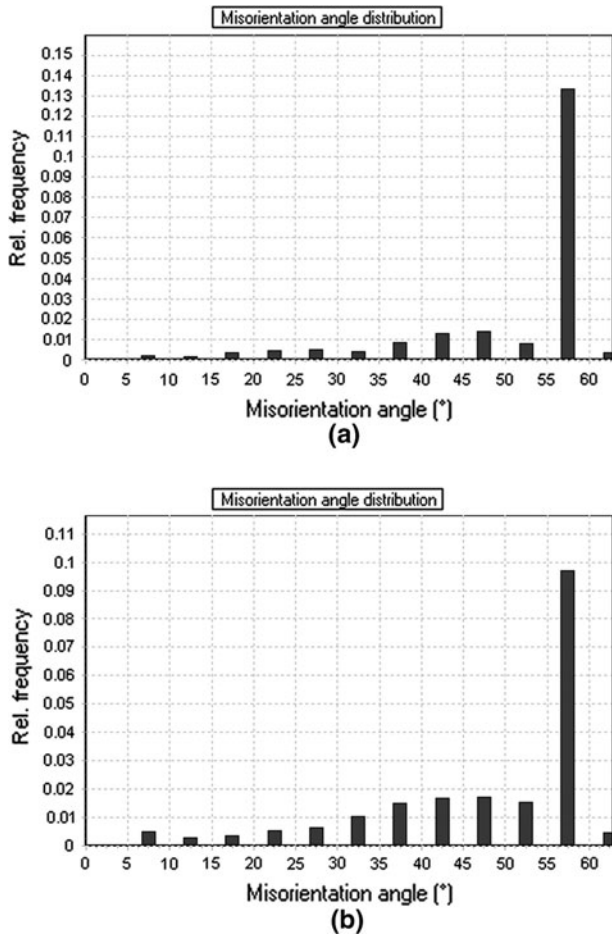


Fig. 5—Misorientation angle distribution (a) As-received AISI 304 and (b) friction surfaced AISI 304 coating.

formation and migration of high angle grain boundaries driven by the stored energy due to plastic deformation.^[10] The strain rate and the temperature involved in the process are the controlling parameters in grain size evolution during DRX.^[11] The dependence of strain rate and temperature are usually represented by the Zener Holoman parameter, Z , which is given as

$$Z = \dot{\epsilon} \left(\exp \left(\frac{Q_c}{RT} \right) \right) \quad [1]$$

where $\dot{\epsilon}$ is the strain rate, Q_c is the activation energy for self diffusion, R is the universal gas constant, and T is the temperature. In most of the hot working process, strain rate is a controllable parameter. However, in friction stir welding/friction stir processing and friction surfacing, which can be considered as hot working processes, the strain rate is not a controllable parameter. In such a situation, the strain rate may be derived based on a torsion type deformation equation.^[12]

$$\dot{\epsilon} = \frac{R_m * 2\pi r_e}{L_e} \quad [2]$$

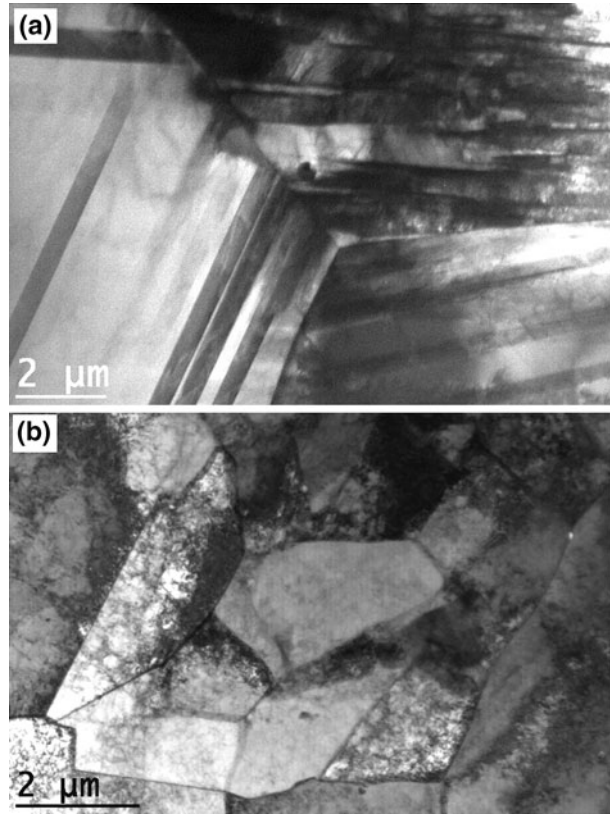


Fig. 6—TEM bright field image (a) as-received AISI 304 and (b) friction surfaced AISI 304 coating.

where r_e and L_e are the effective (or average) radius and depth, respectively, of the dynamically recrystallized zone. In the case of friction surfacing, the effective radius, r_e , that can represent the average radius for all parts of the materials inside this zone, is assumed to be equal to about the diameter of the consumable rod. Similarly, the effective depth of DRX zone, L_e , can be assumed to be equal to the thickness of the coating. R_m is the average material flow rate which can be assumed to be about half the consumable rotational speed. The material flow during friction surfacing is mostly controlled by the rotation speed of the consumable rod.^[13] Hence, the material flow rate may be compatible to or lower than the rotational speed of the rod since there would be a certain level of rotation lagging effect. Therefore, it is reasonable to assume that the material flow rate was about half of the consumable rod rotational speed.

In metals in which the recovery process is slow, such as those with a low or medium stacking fault energy (copper, nickel, and austenitic iron), dynamic recrystallization takes place when a critical deformation condition is achieved.^[14] Most of the severe plastic deformation processes such as equal channel angular pressing (ECAP) and high pressure torsion (HPT) operate at low strain rates of less than 10 s^{-1} .^[15-17] However, strain rates as high as 100 s^{-1} are used in hot rolling mills.^[18] During friction surfacing, the effective strain rate is expected to be above 100 s^{-1} (based

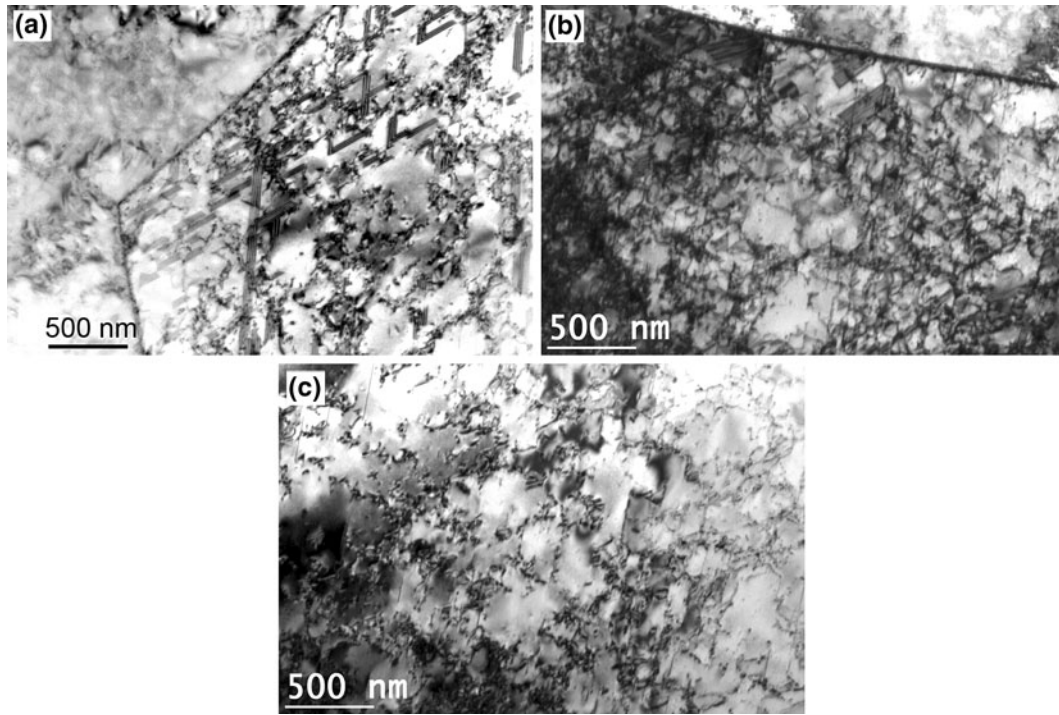


Fig. 7—TEM bright field image from different locations of friction surfaced AISI 304 coating showing substructure evolution.

on torsion type deformation equation), which exceeds the critical strain rate to initiate dynamic recrystallization.

Discontinuous dynamic recrystallization process starts with the nucleation of new grains at the existing grain boundaries through a process called “necklacing”.^[19] A continuous strand of new grains forms along the existing grain boundary and, further, it propagates inward to the grain by subsequent nucleation of new grains at the boundaries of the growing grains. As the material continues to deform, the dislocation density of the new grains increases, thus reducing the driving force for their further growth. Eventually, the entire existing grain will get fully occupied by the newly formed grains and the material will become fully recrystallized. Complete recrystallization happens only at relatively large accumulated strains. If the recrystallization is not complete, then the resulting microstructure would exhibit a “necklace” like feature. The TEM as well as OIM images of the friction surfaced coating did not show any necklace features, which indicates that the coating microstructure had undergone complete recrystallization.

Yet another possible DRX mechanism that might have played a role in completing the recrystallization process could be metadynamic recrystallization.^[20] Whenever the critical strain for dynamic recrystallization is exceeded, recrystallization nuclei will be present in the material. When straining is stopped, but annealing is continued, these nuclei will grow with no incubation period into the heterogenous partly dynamically recrystallized matrix. In the current work, however, no conclusive evidence is obtained to show the occurrence of such a mechanism.

In summary, the grain evolution during friction surfacing may be compared to that for the discontinuous DRX occurring during hot working processes. Since friction surfacing involves very high strain rates, critical dislocation densities required for the initiation and completion for discontinuous DRX can be easily achieved. Hence, the metallic coatings made by friction surfacing can result in very fine wrought microstructures which can significantly improve the performance of the coating.

IV. CONCLUSIONS

AISI 304 coatings produced by friction surfacing are microstructurally characterized to understand the evolution of microstructure. The severe plastic deformation involved in the friction surfacing process resulted in dynamically recrystallized AISI 304 coating microstructure. The grain refinement in the coating due to discontinuous DRX was found to be in the order of 3 to 8 μm . The fine-grained microstructure was free from carbides or any secondary phases, which implies that the material properties will remain unaltered during friction surfacing.

ACKNOWLEDGMENTS

The authors would like to thank the Naval Research Board, Ministry of Defense, Govt. of India for funding this work.

REFERENCES

1. V.I. Vitanov and I.I. Voutchkov: *J. Mater. Process. Technol.*, 2005, vol. 159, pp. 27–32.
2. A.W. Batchelor, S. Jana, C.P. Koh, and C.S. Tan: *J. Mater. Process. Technol.*, 1996, vol. 57, pp. 172–81.
3. M. Chandrasekaran, A.W. Batchelor, and S. Jana: *J. Mater. Process. Technol.*, 1997, vol. 72, pp. 446–52.
4. G.M. Reddy and T. Mohandas: *Proceedings of the International Institute of Welding International Congress 2008*, Chennai, India, 8–10 January 2008, pp. 1197–1213.
5. G.M. Bedford, V.I. Vitanov, and I.I. Voutchkov: *Surf. Coat. Technol.*, 2001, vol. 141, pp. 34–39.
6. T. Ishida: *J. Mater. Sci.*, 1991, vol. 26, pp. 6431–35.
7. V.I. Vitanov, I.I. Voutchkov, and G.M. Bedford: *J. Mater. Process. Technol.*, 2000, vol. 107, pp. 236–42.
8. D. Govardhan, A.C.S. Kumar, K.G.K. Murti, and G.M. Reddy: *Mater. Des.*, 2012, vol. 36, pp. 206–14.
9. H.K. Rafi, G.D.J. Ram, G. Phanikumar, and K.P. Rao: *World Congress on Engineering (WCE-2010)*, London, U.K., 30 June–2 July 2010.
10. R.D. Doherty, D.A. Hughes, F.J. Humphreys, J.J. Jonas, D.J. Jensen, M.E. Kassner, W.E. King, T.R. McNelley, H.J. McQueen, and A.D. Rollett: *Mater. Sci. Eng. A*, 1997, vol. 238, pp. 219–74.
11. A. Belyakov, K. Tsuzaki, H. Miura, and T. Sakai: *Acta Mater.*, 2003, vol. 51, pp. 847–61.
12. C.I. Chang, C.J. Lee, and J.C. Huang: *Scripta Mater.*, 2004, vol. 51, pp. 509–14.
13. H.K. Rafi, G. Phanikumar, and K.P. Rao: *Metall. Mater. Trans. A*, 2011, vol. 42A, pp. 937–39.
14. F.J. Humphery and M. Hatherly: *Recrystallization and Related Annealing Phenomena*, Elsevier Sciences Ltd., Oxford, U.K., 1996.
15. H. Beladi, G.L. Kelly, and P.D. Hodgson: *Int. Mater. Rev.*, 2007, vol. 52, pp. 14–28.
16. H.B. Mcshane and T. Sheppard: *J. Mech. Work. Technol.*, 1984, vol. 9, pp. 147–160.
17. A. Dehghan-Manshadi and P.D. Hodgson: *ISIJ Int.*, 2007, vol. 47 (12), pp. 1799–1803.
18. J.A. DeAlmeida and B. Barbosa: *ISIJ Int.*, 2005, vol. 45, pp. 296–98.
19. D. Ponge and G. Gottstein: *Acta Mater.*, 1998, vol. 46 (1), pp. 69–80.
20. H. Beladi, P. Cizek, and P.D. Hodgson: *Scripta Mater.*, 2010, vol. 62, pp. 191–96.